

# Membrane Potential Fluctuations Determine the Precision of Spike Timing and Synchronous Activity: A Model Study

JUTTA KRETZBERG, MARTIN EGELHAAF AND ANNE-KATHRIN WARZECHA  
*Lehrstuhl für Neurobiologie, Fakultät für Biologie, Universität Bielefeld, Postfach 10 01 31,  
D-33501 Bielefeld, Germany*  
ak.warzecha@biologie.uni-bielefeld.de

*Received February 23, 2000; Revised August 9, 2000; Accepted August 24, 2000*

Action Editor: Christof Koch

**Abstract.** It is much debated on what time scale information is encoded by neuronal spike activity. With a phenomenological model that transforms time-dependent membrane potential fluctuations into spike trains, we investigate constraints for the timing of spikes and for synchronous activity of neurons with common input. The model of spike generation has a variable threshold that depends on the time elapsed since the previous action potential and on the preceding membrane potential changes. To ensure that the model operates in a biologically meaningful range, the model was adjusted to fit the responses of a fly visual interneuron to motion stimuli. The dependence of spike timing on the membrane potential dynamics was analyzed. Fast membrane potential fluctuations are needed to trigger spikes with a high temporal precision. Slow fluctuations lead to spike activity with a rate about proportional to the membrane potential. Thus, for a given level of stochastic input, the frequency range of membrane potential fluctuations induced by a stimulus determines whether a neuron can use a rate code or a temporal code. The relationship between the steepness of membrane potential fluctuations and the timing of spikes has also implications for synchronous activity in neurons with common input. Fast membrane potential changes must be shared by the neurons to produce synchronous activity.

**Keywords:** spike mechanism, model, spike timing, synchronization, reliability, neural coding

## 1. Introduction

Spike generation appears to be precise, since in many systems spikes occur synchronized in pairs of neurons on a millisecond timescale (e.g., Alonso et al., 1996; Brivanlou et al., 1998; Warzecha et al., 1998; Lampl et al., 1999; Bair, 1999; Usrey and Reid, 1999). Moreover, spikes have been found to be tightly time-locked to fast fluctuations of the membrane potential (Mainen and Sejnowski, 1995; Haag and Borst, 1996; Stevens and Zador, 1998; Zador, 1998).

Despite the precision of the spike-generation mechanism, spikes in sensory neurons couple to stimuli on a broad range of time scales, depending on the sensory

modality and the computational task of the neuron. One extreme are neurons in the auditory and in the electrosensory system that show a precision in spike timing in the millisecond or even submillisecond range (Carr and Friedmann, 1999). In contrast, in the visual system spikes are often found to time-lock to stimuli on a coarser scale (e.g., Buračas et al., 1998; Bair, 1999). For instance, broad-band white-noise velocity fluctuations lead, on average, to a precision in the order of only tens of milliseconds (Warzecha et al., 1998). Nonetheless, a higher precision may be achieved under special stimulus conditions. In motion-sensitive visual neurons rapid displacements of the stimulus pattern may lead to a time-locking of spikes in the millisecond range

(de Ruyter van Steveninck and Bialek, 1988, 1995; Warzecha and Egelhaaf, 2000). On the basis of the experimental results on the time-locking of spikes to sensory stimuli, it has been concluded that a high precision is possible only if the stimuli induce sufficiently rapid depolarizations of the membrane potential. Otherwise, the exact timing of spikes has been proposed to be essentially determined by membrane potential noise (Warzecha et al., 1998).

With a dynamic threshold model of spike generation we tested this hypothesis by analyzing the constraints that are imposed on the time-locking of spikes to membrane potential fluctuations and on correlated spike activity in pairs of cells. In our simulations we took only correlated spike activity into account, which is elicited by common synaptic input rather than by direct synaptic interactions between the neurons. Unlike other studies analyzing the dependence of correlated activity on synaptic input (e.g., Shadlen and Newsome, 1998; Ritz and Sejnowski, 1997), we investigated the relation between the membrane potential of a neuron and its spike output. To tune our model the membrane potential dynamics was taken from intracellular recordings of postsynaptic potentials of a fly motion-sensitive neuron that responds with graded membrane potential changes to motion stimuli even in its output terminal. The model output was compared to experimental data from a spiking neuron with functionally similar properties. Since identified motion-sensitive neurons in the fly are well amenable to electrophysiological analysis, the fly has been used previously to investigate the neuronal processing of motion information and its reliability (Hausen, 1981; Bialek and Rieke, 1992; Egelhaaf and Warzecha, 1999).

By modeling the transformation of membrane potential fluctuations into sequences of spikes, we answer the following questions: What characteristics of the membrane potential and, in particular, what aspects of its dynamics determine the timing of spikes? To what extent do the postsynaptic potentials of two cells have to correspond to one another to cause synchronized spike activity?

## 2. Methods

To investigate the determinants of the timing of spikes we used a phenomenological threshold model that transforms the time-dependent membrane potential into a sequence of spikes. For each time step a variable threshold was calculated and compared to the actual

membrane potential to determine whether a spike was generated.

To tune the model and to compare the model output with experimentally determined spike trains, the membrane potential dynamics was taken from experimental data. For systematic analyses sinusoidal membrane potential fluctuations were used. To simulate many experimental trials with the same stimulus (such as a visual motion stimulus or current injection), a stochastic component that differed for each trial was superimposed onto the deterministic component of the membrane potential fluctuations (Fig. 1). The deterministic component is given by the mean time-dependent membrane potential fluctuations evoked by a given stimulus. The stochastic component accounts for the variability of neuronal responses.

All our analyses are based on the assumption that the stochastic response component adds linearly to the deterministic component. We are currently investigating whether this assumption applies to motion-sensitive neurons in the fly (Warzecha et al., 2000) since for retinal ganglion cells model simulations indicate the opposite (Levine, 1998).

### 2.1. Dynamical Threshold Model of Spike Generation

The model of spike generation consists of a variable threshold  $\theta(t_i)$  that is compared with the membrane potential  $U(t_i)$ . A spike is generated if  $\theta(t_i) < U(t_i)$ .

The spike threshold was calculated for each time step  $t_i$  according to the equation

$$\theta(t_i) = \begin{cases} \infty & \text{if } s \leq \gamma^{ref} \\ \theta_0 + \eta(s) + \rho(t_i) & \text{if } s > \gamma^{ref} \end{cases},$$

where  $t_i$  is the actual time step,  $s$  is the time elapsed since the previous spike,  $\gamma^{ref}$  is the absolute refractory period,  $\theta_0$  is the constant basis threshold,

$$\eta(s) = \frac{\eta_0}{s - \gamma^{ref}}$$

is the influence of the relative refractoriness with weight constant  $\eta_0$ , and

$$\rho(t_i) = -\frac{\rho_0}{T} \cdot \sum_{j=1}^T \frac{1}{j} \cdot (U(t_i) - U(t_{i-j}))$$

is the influence of the membrane potential changes

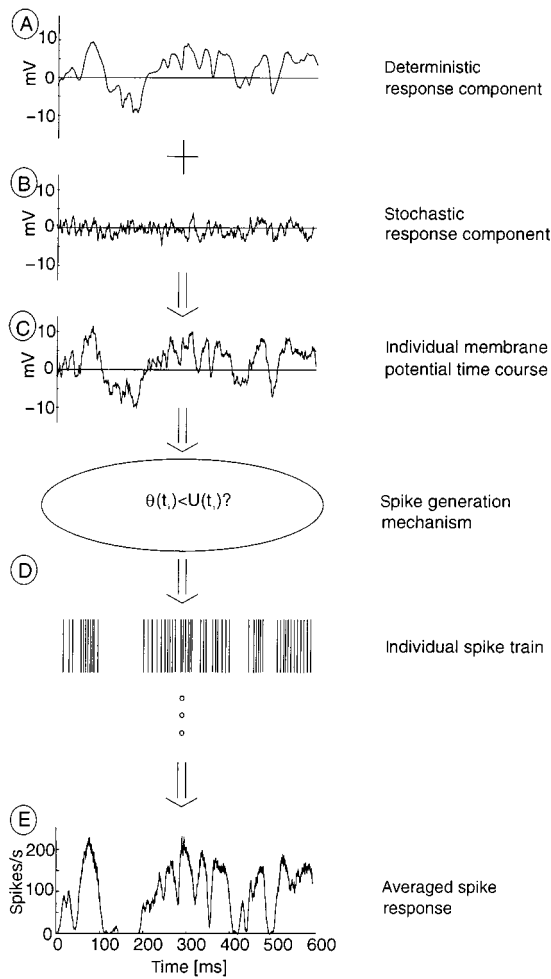


**Figure 1.** Schematic of the model. Membrane potential fluctuations serve as input of the spike generation mechanism. These membrane potential fluctuations consist of two components, a deterministic and a stochastic one. **A:** In the example shown here, the deterministic component corresponds to the averaged membrane potential fluctuations of a visual interneuron of the fly (HS) to dynamic motion stimuli. **B:** The stochastic component differs from trial to trial. It is approximated by low-pass filtered Gaussian white noise that is tuned to the experimentally found variability of neuronal responses. **C:** The sum of stimulus-induced and stochastic component is used as the membrane potential, which is fed into the spike-generation mechanism. **D:** The threshold  $\theta(t_i)$  is calculated for every time step  $t_i$  and compared to the membrane potential value  $U(t_i)$ . If  $\theta(t_i) < U(t_i)$  a spike is generated. **E:** PSTH of model output as obtained from 100 individual responses. For illustration the PSTH is smoothed with a sliding 10 ms rectangular window.

within the last  $T$  data points, with weight constant  $\rho_0$  and the actual membrane potential  $U(t_i)$ .

For a constant membrane potential the term  $\eta(s)$  causes the threshold to decrease to the constant value  $\theta_0$

after the absolute refractory period  $\gamma^{ref}$ . When the membrane potential varies, the resulting threshold is influenced by the term  $\rho(t)$ . It represents the weighted and sign-inverted sum of the slopes between the last  $T$  membrane potential values and the reference potential  $U(t_i)$  at time  $t_i$ . The threshold decreases while the membrane potential depolarizes, and it rises while  $U(t)$  hyperpolarizes. The steeper the membrane potential rises or falls, the more the threshold is influenced by the term  $\rho(t)$ . This term has been included in the model because fast rises in membrane potential were experimentally found to be more effective in eliciting a spike than slow ones (e.g., Johnston and Wu, 1995). Table 1 specifies the parameter sets that were used to simulate spike responses of a motion-sensitive cell of the fly (see also Section 2.2, Tuning of the Model).

In contrast to many other model approaches we did not make any assumptions about the origin of the membrane potential fluctuations,—that is, about the statistics of the activity of the presynaptic neurons, about synaptic transmission, and about dendritic integration. Rather membrane potential fluctuations were taken as input for the spike-generation mechanism as they have been determined experimentally in motion-sensitive neurons of the fly, no matter what cellular processes were involved in their generation. For integrate-and-fire models (for an overview of different types of integrate-and-fire models, see, e.g., Softky and Koch, 1993; Maass, 1996; Koch, 1999) the integration of synaptic input and spike generation are usually combined. If the terms that reflect in our model the dependence of the spike threshold on the relative refractoriness and the membrane potential changes ( $\eta(s)$  and  $\rho(t)$ ) are set to zero, the spike generation in our model is identical to that of an integrate-and-fire model with a constant refractory period.

In a previous study (Warzecha et al., 1998) we used a different model than is used here for simulating the correlated activity of pairs of neurons in the fly's brain. Our previous model dealt with spike probabilities depending on a variable threshold. It included relative refractoriness but did not explicitly take into account the influence of membrane potential changes. Although this model could reproduce relevant features of the correlated output of the two neurons, we decided to use a model that generates spikes deterministically. Instead of a stochastic spike generation mechanism we introduced in the present approach stochastic membrane potential fluctuations as they are induced by stochastic synaptic input, channel noise, and thermal noise

*Table 1.* Ranges for tested parameter values and examples for parameter sets that fit all criteria to simulate the H1-cell. Parameter set number 1 was used as standard parameter set.

	$\theta_0$ (mV)	$\gamma^{ref}$ (ms)	$\eta_0$ (ms·mV)	$\rho_0$	$T$
Tested range	−2–5	0–2	0–60	0–200	0–40 (corresp. $\approx$ 15 ms)
Set 1	1	2	20	3.75	3 (corresp. $\approx$ 1 ms)
Set 2	0	0	40	3	3 (corresp. $\approx$ 1 ms)
Set 3	3	1	20	9	6 (corresp. $\approx$ 2 ms)
Set 4	1	1	30	7.5	12 (corresp. $\approx$ 4 ms)
Set 5	0.5	0.5	25	0	0

(see, e.g., Manwani and Koch, 1999a, 1999b). Ion channel stochasticity may contribute significantly to the variability of spike timing (e.g., Schneidman et al., 1998; White et al., 2000). Nevertheless, there is evidence that in many situations the stochastic nature of the mechanisms underlying spike generation contributes much less to the variability in the timing of spikes than membrane potential fluctuations that are conveyed to a neuron by its synaptic input but are not locked to its sensory input (see Mainen and Sejnowski, 1995; Zador, 1998; Stevens and Zador, 1998). Therefore, a deterministic model is appropriate for our analyses.

The model simulations and all evaluation routines were implemented in Matlab 5.3 (The MathWorks Inc.). A temporal resolution of 2.7 kHz was used for the model of spike generation.

## 2.2. *Tuning of the Model*

To find appropriate parameter values, we compared the simulation results directly with experimentally determined spike trains of the H1-cell, a motion-sensitive visual interneuron of the fly (Hausen, 1981). The visual system of the fly is well suited for our analysis because it contains at the same level of information-processing spiking neurons (such as the H1-cell) as well as neurons that respond with graded membrane potential changes (such as the HS-cells) even in the neuronal output region. These graded membrane potential changes mainly reflect the integrated postsynaptic potentials of the cell's many retinotopically organized inputs.

The H1-neuron receives similar retinotopic input and is assumed to respond with graded membrane potential changes in a similar way as the HS-cells when the activity is recorded intracellularly in its dendritic tree. Since intracellular recordings of the H1-neuron

are very difficult because of the small diameter of all of the H1-cell's dendritic branches, the graded membrane potential changes of the HS-cells were used as a substitute for those of the H1-cell and fed as input into the spike-generation mechanism. To use the membrane potential of the HS-cell has also the advantage that it is less influenced by active processes than the one of the H1-cell. Therefore, it better reflects the integrated postsynaptic potential.

To substitute the postsynaptic potential of the H1-cell by that of the HS-cell is justified because both types of neurons show functionally similar properties without having direct synaptic connections with each other (for review, see Egelhaaf and Warzecha, 1999). For instance, for a wide range of motion stimuli the time course of the stimulus-induced response component of HS-cells, as obtained by averaging over many responses to repeated stimulus presentations (Fig. 2A), is very similar to the stimulus-induced responses of the H1-neuron as reflected in its peri-stimulus-time histogram (PSTH, Fig. 2B). The relation between membrane potential changes in the HS-neuron and spike timing in the H1-cell was further characterized by the spike-triggered average of the membrane potential (Fig. 2C).

This analysis was done for responses obtained from double recordings of the HS-cell and the H1-cell. Responses were correlated with each other that were either simultaneously recorded or randomly assorted (shuffled). Both spike-triggered averages are characterized by a fairly broad and large peak, suggesting that the neuronal responses are time-locked to the motion stimulus on a timescale of some tens of milliseconds. The difference between these two spike-triggered averages (Fig. 2D) indicates that, on a finer timescale, both neurons also share parts of their input signals that are not deterministically coupled to the stimulus but vary from trial to trial. It should be noted that the response traces of the HS-cells had to be sign inverted for

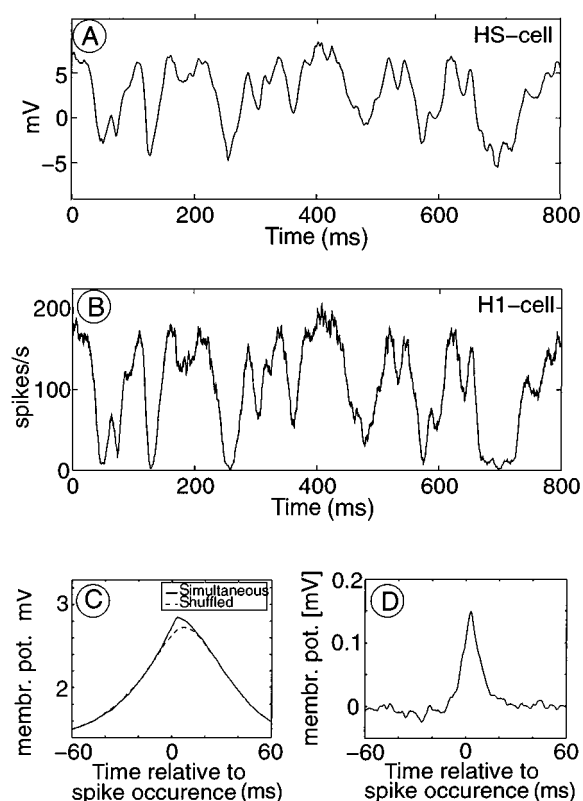


**Figure 2.** Comparison of the membrane potential of an HS-cell and the spike activity of the H1-cell. The activity of both neurons was recorded during stimulation with lowpass-filtered white-noise velocity fluctuations. The resting potential of the HS-cell was set to zero and the membrane potential was sign-inverted to account for the opposite preferred directions of the HS-cell and the H1-cell. **A**, **B**: Average time course of the membrane potential of the HS-cell and of the spike activity of the H1-cell to identical motion stimuli. The mean responses to 100 stimulus presentations for each cell were smoothed with a sliding rectangular window of 10 ms width. Stimulus conditions were the same as in Warzecha et al. (1998, Fig. 3). The membrane potential of the HS-cell and the spike activity of the H1-cell show a very similar time course. Recordings of the HS-cell and the H1-cell were performed in different animals. **C**: Mean membrane potential of an HS-cell triggered at time 0 with the spikes of the H1-cell obtained from a double recording of both cells with 49 stimulus presentations. The analyzed time interval lasted for 3.1 s. The mean spike activity within this interval was 85 spikes/s. Spike-triggered averages are shown for simultaneously recorded responses (solid line) and for the same response traces that were assorted in shuffled order so that response traces were combined that were not measured simultaneously (dashed line). **D**: Difference between the spike-triggered mean membrane potential of the simultaneously recorded and the shuffled responses. Same data as those shown in C.

comparison with the spike response of the H1-cell and when feeding them into the model cell because the H1- and the HS-cells have opposite preferred directions.

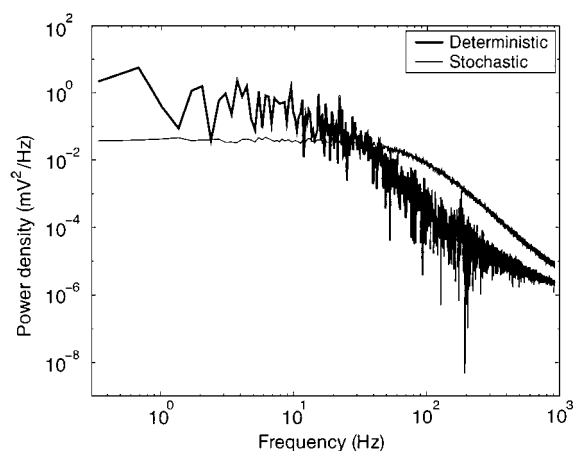


**Figure 3.** Power spectrum of the deterministic membrane potential component (thick line) in response to low-pass-filtered white-noise velocity fluctuations and average spectrum of the stochastic membrane potential component (thin line) simulated by low-pass-filtered Gaussian white noise. The deterministic component was obtained by averaging 100 experimentally recorded individual responses to the same motion stimulus and lasted 2.96 s. The power spectrum of the stochastic component was obtained by averaging the spectra of 100 artificially generated stochastic membrane potential components of the same duration. It was fitted to the power spectrum of the experimentally determined stochastic membrane potential component shown in Warzecha et al. (1998, Fig. 3D).

The membrane potential traces used to tune the model consisted of two components (Fig. 1):

- The *deterministic component of the membrane potential* was determined as the time-dependent membrane potential of the HS-cell averaged over 100 responses to identical dynamical motion stimulation. The averaging was assumed to eliminate the stochastic component and therefore to represent the stimulus-induced response component. For motion stimulation with white-noise velocity fluctuations the stimulus-induced component of the membrane potential has most power below 20 Hz (Fig. 3 and Haag and Borst, 1997; Warzecha et al., 1998). The deterministic membrane potential trace we used to tune the model had a duration of 2.96 s and a variance of  $13.2 \text{ mV}^2$ .
- The *stochastic component of the membrane potential* was computed individually for each trial as a series of lowpass-filtered Gaussian distributed random numbers. The distribution of the membrane potential noise can be well approximated by a Gaussian distribution (see also Hengstenberg, 1982; Haag and Borst, 1997; Warzecha et al., 2000). By low-pass filtering the power spectrum of the stochastic

component was fitted to the power spectrum of the experimentally determined membrane potential noise of an HS-cell recorded during white-noise velocity stimulation (Fig. 3 and Warzecha et al., 1998). We used a second-order lowpass filter with equal time constants of 1.6 ms. The variance of the stochastic component was set to  $2.8 \text{ mV}^2$  in accordance with experimental data. The stochastic component of the membrane potential has considerably more power at frequencies above 40 Hz than the stimulus-induced deterministic component (Fig. 3 and Warzecha et al., 1998).

The deterministic and the stochastic components of the membrane potential were added and then fed into the

spike-generation mechanism. This was done for 100 different stochastic sequences. The model was tuned with membrane potential fluctuations elicited by dynamic motion stimuli. A set of model parameters was accepted if the model responses were sufficiently similar to the H1-cell responses obtained with the same dynamic motion stimuli. The similarity was assessed according to the following criteria:

- *Mean spike count*: The mean simulated spike response had to be between 80 spikes/s and 105 spikes/s, which was the range of mean activities found in different H1-cells.
- *Peristimulus-time histogram (PSTH)*: PSTHs were determined from 100 responses of both the H1-cell

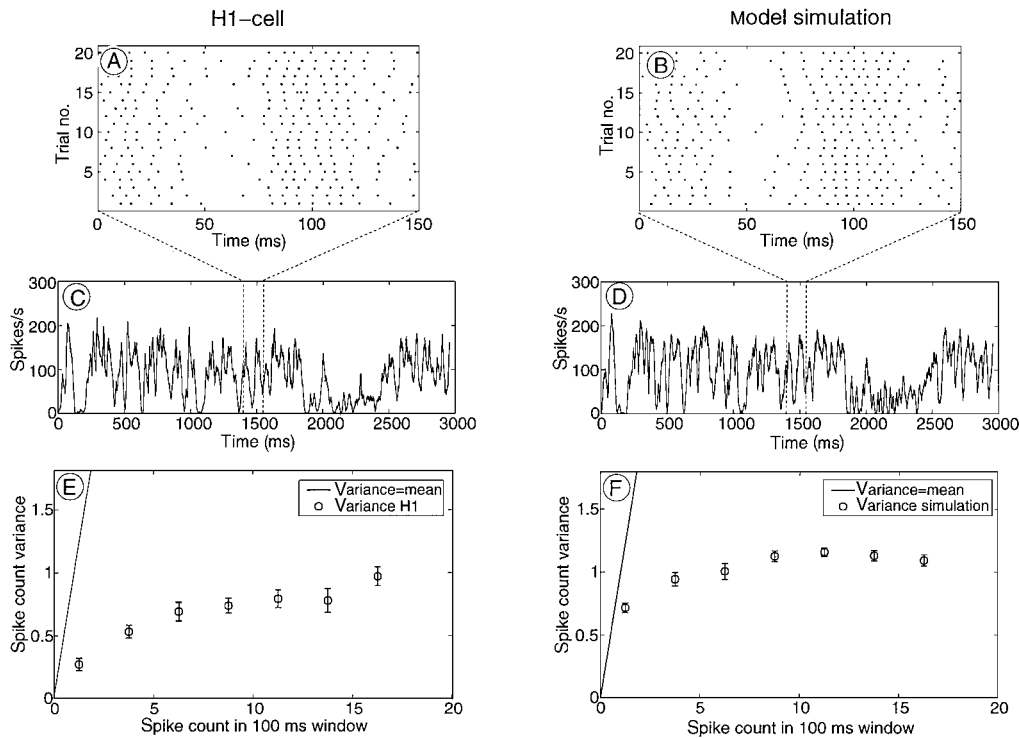


**Figure 4.** Comparison of experimental data and model simulations. The deterministic membrane potential fluctuations that were used as input of the model were obtained from intracellular recordings from an HS-cell. The HS-cell was stimulated with the same white-noise velocity fluctuations as were used when the spike activity of the H1-cell was recorded. **A, B:** Raster plots of 20 response traces of the H1-cell (**A**) and of the model (**B**). Rasters show a section of the response illustrated by the PSTHs in **C, D** (see dashed lines). **C, D:** PSTH of responses of the H1-cell (**C**) and of the model (**D**). For both PSTHs, 100 individual responses were averaged and smoothed with a sliding 10 ms rectangular filter. Coefficient of correlation between both PSTHs: 0.93. **E, F:** Variance of the spike count as a function of the mean spike count. Spikes were counted within 100 ms time intervals. Consecutive time intervals overlapped by 90 ms. The mean spike-count values were assigned to activity classes with a width of 2.5 spikes per 100 ms. Spike-count variances associated with mean spike counts that fell into the same activity class were averaged. Responses of the H1-cell and the stimulus-induced membrane potential of the HS-cell, which was used as input of the model, were elicited by low-pass-filtered white-noise velocity fluctuations with the same statistical properties. For both the experimental data and the model simulations the variance does not equal the mean spike count (solid line). **E:** Error bars denote SEMs of variances across 4 to 8 H1-cells. For each cell 60 individual response traces were evaluated. Modified from Warzecha and Egelhaaf (1999). **F:** Error bars denote SEMs of variance across 10 simulations each consisting of 100 individual response traces.

and the model cell and smoothed with a 10 ms rectangular filter (Fig. 4C and D). To quantify the similarity of their time courses, the correlation coefficient of the smoothed PSTHs was calculated. In accordance to the similarity of PSTHs of H1-cells in different preparations, the correlation coefficient had to reach a value of at least 0.92.

- *Activity distribution*: The mean spike count within time windows of 100 ms duration was determined for the entire spike train (see Fig. 4E and F). Adjacent time windows overlapped by 90 ms. The individual spike count values were assigned to activity classes with a width of 2.5 spikes per 100 ms, and the probability of each activity class was determined. According to experimental data, model parameters were accepted if the model responses satisfied the following criteria: (1) between 1% and 17% of the spike count values had to be in the lowest activity class (0 to 2.5 spikes/100 ms); (2) the activity class that occurred most frequently had to be in the range between 8 spikes/100 ms and 15 spikes/100 ms; (3) between 23% and 30% of the spike count values had to be in the most frequently occurring activity class.
- *Interspike-interval histogram*: The most frequently observed interspike interval had to be between 5 and 8 ms. The frequency of its occurrence had to be between 4% and 10% of all interspike intervals. Interspike intervals were evaluated with a precision of 0.37 ms.

A systematic search was performed with equidistant parameter values for all possible combinations of values within the whole physiologically plausible parameter range (see Table 1). Within the parameter ranges that revealed partly acceptable simulation results, the search was continued with finer subdivisions of the parameter values. Five different parameter sets that satisfied all criteria were chosen for further model analysis (Table 1, sets 1–5). They led to qualitatively the same results. For all figures shown in this article, the standard parameter set 1 was used. In parameter set 5, membrane potential changes are not taken explicitly into account for determining the spike threshold ( $\rho(t) = 0$ ).

### 2.3. Simulation of Spike Timing and Synchronous Activity in Pairs of Cells

Two analyses were performed to investigate the prerequisites of precise spike timing and synchronized activity between pairs of cells. For the analysis of the

*dependence of spike timing on the membrane potential dynamics* the input consisted of two components:

- A sinusoidally fluctuating deterministic input with variable frequency between 1 Hz and 100 Hz and a physiologically plausible amplitude of 5.1 mV;
- A stochastic component with the shape of its power spectrum fitting that of the HS-cell under white-noise velocity stimulation (see Section 2.2, Tuning of the Model) and with the same or half of its variance.

For analyzing the *dependence of spike synchronization on the amount of common input* the input of pairs of model cells consisted of three components:

- The deterministic component of the membrane potential of the HS-cell obtained during dynamical motion stimulation (see Section 2.2, Tuning of the Model) (this component was common to both cells);
- A stochastic component that was shared by both cells and that represents common input that is not deterministically induced by the stimulus;
- A stochastic component that was statistically independent for both cells simulating intrinsic noise of the cell and all input that is not shared by both cells.

The power spectrum and the variance of the total stochastic component ( $\langle S_{tot}^2 \rangle$ ) consisting of the common and the independent component were fitted to that determined for the HS-cell (see Section 2.2, Tuning of the Model). To estimate the influence of the common stochastic input on the extent of correlated activity, the relative size of the two stochastic components was varied keeping the shape of their power spectrum unaltered. Each stochastic component was generated separately as described above. The common and the independent stochastic component were scaled to have the variances  $\langle S_c^2 \rangle$  and  $\langle S_i^2 \rangle$ , respectively, with

$$\langle S_c^2 \rangle + \langle S_i^2 \rangle = \langle S_{tot}^2 \rangle = const$$

—that is, the total variance was held constant at the experimentally determined value. The common stochastic input will be given as a relative measure ( $C$ ).  $C$  is calculated as the percentage of the standard deviation of the common stochastic component relative to the sum of the standard deviations of the common and the independent stochastic components:

$$C = 100 \cdot \frac{\sqrt{\langle S_c^2 \rangle}}{\sqrt{\langle S_i^2 \rangle} + \sqrt{\langle S_c^2 \rangle}}.$$

To quantify the similarity of individual spike trains, cross-correlograms were calculated that were normalized to the respective autocorrelograms, so that for identical spike trains a value of 1.0 is obtained at zero lag. The height of the correlation peak was defined as the relative frequency of coincidences above the chance level of spike coincidences in the two cells. The chance level was calculated on the basis of the mean activity of both cells. Note that the subtraction of the chance level causes the maximum correlation height to be smaller than 1 even for identical spike trains. The correlation width was calculated at half-maximum height above chance level. All cross-correlations were computed with a temporal resolution of 1.1 ms as it was used for the corresponding experimental data.

It has been argued that the cross-correlogram of responses to repeated presentations of the same stimulus is no valid measure to quantify the precision with which spikes time-lock to the stimulus. Rather, the precision of time-locking should be quantified by deconvolution of the cross-correlogram by the corresponding autocorrelogram of the responses (de Ruyter van Steveninck et al., 2000). However, the resulting autocorrelogram of the spike jitter distribution indicates a high precision of time-locking of spikes to the stimulus, only if the spike jitter is considerably smaller than half the interspike interval. The spike jitter is given by the variable timing of spikes in different trials relative to a given instant of time. If, for instance, spikes are generated at an average rate of 200 spikes/s, the mean interspike interval is 5 ms. In this case a jitter in the timing of spikes of only a few milliseconds would be an immediate consequence of the relatively high spike rate without indicating that the spikes are precisely time-locked to the stimulus. The cross-correlogram of responses elicited by repeated presentation of the same stimulus would then be rather flat. In contrast, if spikes, on average, lock to stimuli with a spike jitter smaller than about half the interspike interval, this precision will show up in a narrow peak of the cross-correlogram. Therefore, cross-correlograms will be used in the present analysis to quantify the similarity of spike trains and, thus, the time-locking of spikes to sensory stimulation. It should be noted that cross-correlograms are only a measure of the *overall* precision and that a broad cross-correlogram does not exclude that part of the spikes are generated with a high precision at *certain* phases of a stimulus trace (Warzecha and Egelhaaf, 2000).

Moreover, cross-correlograms will be used to quantify synchronized spike activity of pairs of neurons.

It has been argued that this method is questionable if the width of the correlograms are in the same order of magnitude as the peak width of the autocorrelogram of the PSTHs (Brody, 1999). In our simulations as well as in our experimental results (Warzecha et al., 1998) this is not the case. The simultaneously elicited spike activity is synchronized on a time scale of single milliseconds, while the covariation of the cell's activities induced by the stimulus concerns a time scale of some tens of milliseconds. This can be seen in the PSTHs as well as the shuffled cross-correlogram of spike responses that show a broad ( $\sim 30$  ms) and flat peak. In contrast, the peak of the cross-correlogram of simultaneously recorded spike responses is narrow ( $\sim 2$  ms) and high (Warzecha et al., 1998; Figs. 2 and 7 in this article).

### 3. Results

#### 3.1. Comparison of Model Simulations and Experimental Results

The spike-generation model reproduces characteristic response features of the fly motion-sensitive H1-cell, when it is fed with membrane potential fluctuations as were determined experimentally in a neuron with similar response properties (an HS-cell). Various sets of model parameters (Table 1) were found to meet the criteria for accepting the model responses as an adequate fit to the corresponding neuronal responses (see Section 2, Methods). For some parameter sets membrane potential changes did not explicitly affect the spike threshold because the term  $\rho(t)$  was set to zero ( $\rho_0 = 0$  or  $T = 0$ ; see set 5 in Table 1). It has not been possible to fit model responses to experimental data when the relative refractory period  $\eta_0$  was set to 0. In this case the interspike-interval histograms had a sharp peak that was much larger than was found experimentally. Thus, the criteria employed to tune the model to response properties of the H1-cell of the fly could not be satisfied with a constant threshold as it is used in standard integrate-and-fire models.

The close correspondence of the experimentally determined and the simulated data is illustrated in Fig. 4 for three response features. The PSTH of the model responses was found to be very similar to the PSTH determined from the responses of the H1-cell to the same white-noise velocity fluctuations that elicited the membrane potential used as deterministic input to the model (Fig. 4C and D). Judged by the correlation

coefficient (see Section 2, Methods) both PSTHs were as similar as PSTHs of different H1-cells.

The model does not only account for the cellular responses as averaged over many stimulus presentations. For individual spike trains it is impossible to tell whether they represent the output of the model or of the H1-cell (Fig. 4A and B). The model also reproduces the variability of the neuronal responses as quantified by the across-trial variance of the spike count. It should be noted that the model has not been adjusted to fit the experimentally determined variance of neuronal responses. In Fig. 4E and F the mean spike count variance determined within time windows of 100 ms from responses to dynamic velocity stimulation is plotted versus the mean spike count determined within the corresponding time windows. For both, the H1-neuron and the model, the variance does not increase much with increasing mean spike count for large parts of the cells' activity range (for details concerning the experiments, see Warzecha and Egelhaaf, 1999; for a detailed analysis of spike count variances of the H1-cell and model responses, see Warzecha et al., 2000). Hence, for levels of stochastic membrane potential fluctuations as found in intracellular recordings of fly motion-sensitive neurons the spike count variance remains much smaller than the mean spike count. Although this finding is not restricted to fly motion-sensitive neurons (see e.g., Berry et al., 1997), it is by no means trivial, given the fact that the variance of many neurons was found to increase about linearly with the mean activity (e.g., Tolhurst et al., 1983; Vogels et al., 1989; Britten et al., 1993).

Hence, although only the averaged time course of the spike response and the interspike interval histogram were included into the parameter evaluation (see Section 2, Methods), the model is also capable of reproducing the variability of responses of a fly motion-sensitive neuron. Therefore, we used the model to analyze general aspects of the time-locking of action potentials to membrane potential fluctuations and the correlated activity of pairs of nerve cells.

### 3.2. *Dependence of Spike Timing on the Membrane Potential Dynamics*

We analyzed systematically how the dynamics of membrane potential fluctuations influences the precision of spike generation. For this purpose, sinusoidal membrane potential fluctuations were used as

the deterministic component instead of the stimulus-induced responses obtained from real neurons. The sinusoidal deterministic membrane potential fluctuations were superimposed with stochastic fluctuations that differed for each trial. The shape of the power spectrum of the stochastic fluctuations was fitted to the one determined experimentally for white-noise velocity stimulation (see Section 2, Methods, and Fig. 3).

The PSTH of the simulated cell obtained with a 5 Hz input is virtually sinusoidal except for clipping at low rates and, thus, resembles strongly the deterministic input (Fig. 5A). A spike can be generated at any time when the membrane potential is sufficiently depolarized. The probability for eliciting a spike increases with increasing depolarization of the cell. The spikes do not time-lock on a millisecond timescale to the sinusoidal input at this frequency. Rather, the exact timing of spikes depends on the stochastic membrane potential changes. For such low input frequencies the spike rate is basically proportional to the deterministic membrane potential which is fed into the spike generation mechanism. For a 30 Hz input (Fig. 5B) the PSTH is no longer sinusoidally modulated but shows several short peaks during each depolarization phase. The individual spikes begin to phase-lock to the sinusoidal fluctuations of the deterministic membrane potential component. Fluctuations of the input at 80 Hz cause a very precise time-locking of spikes. Accordingly, the resulting PSTH shows sharp peaks (Fig. 5C). Additional small peaks in the PSTH indicate that a second spike is occasionally generated within one cycle. For higher frequencies the small peaks disappear and only one spike is generated for each cycle with a jitter below one millisecond. If the input frequency is high enough to cause peaks in the PSTH, the first and largest peak occurs for each depolarization phase before the maximum of the depolarization is reached indicating a phase shift between the spike rate and the deterministic sinusoidal input.

For a quantitative analysis of the temporal precision of spike timing, we calculated the cross-correlogram of individual spike trains. For this analysis two different parameter sets and two levels of the stochastic component were used (see legend of Fig. 6). The height of the cross-correlogram above the chance level of spike coincidences and the width of the correlogram at half height were used as measures of the similarity of individual spike trains and, thus, of the precision with which the spikes time-lock to the deterministic membrane potential component. For both levels

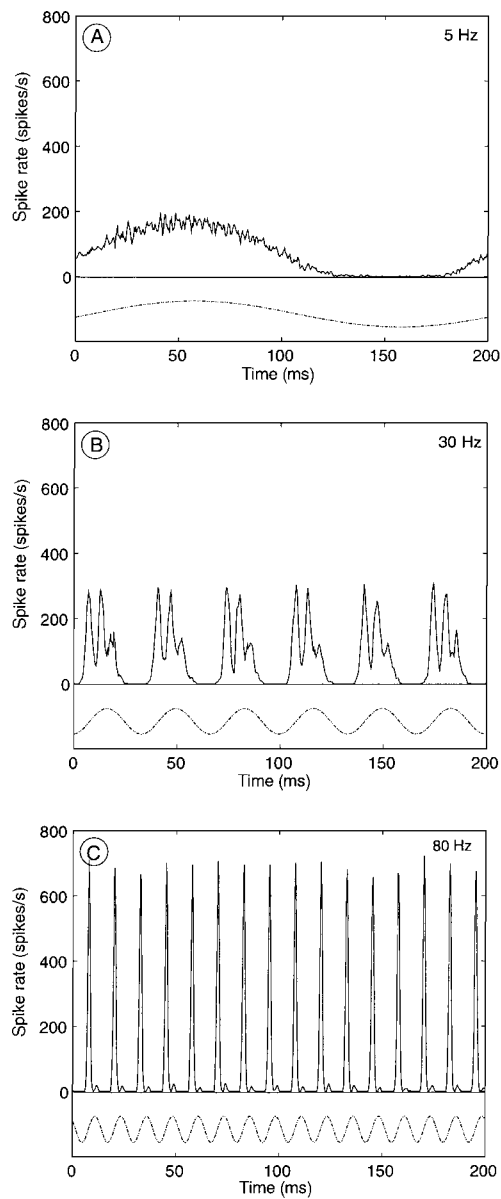


**Figure 5.** Time-locking of spikes to sinusoidal membrane potential fluctuations. The deterministic component of the membrane potential that was fed into the model cell fluctuated sinusoidally with an amplitude of 5.1 mV around a mean of 1.89 mV. For each trial the sinusoidal fluctuations were superimposed by different stochastic fluctuations with a variance of  $1.4 \text{ mV}^2$ . Three examples of PSTHs for sinusoidal input oscillating at a low (A: 5 Hz), a medium (B: 30 Hz), and a high (C: 80 Hz) frequency are shown. PSTHs were computed with a temporal resolution of 0.37 ms using the standard parameter set. They were averaged over 500 trials and smoothed with a running average of 1.1 ms. The sinusoidal membrane potential fluctuations (dotted lines) used as stimulus-induced input to the spike-generation mechanism is shown below the PSTHs (solid lines). The variance of the stochastic fluctuations was half the size of that determined for the HS-cell responses.

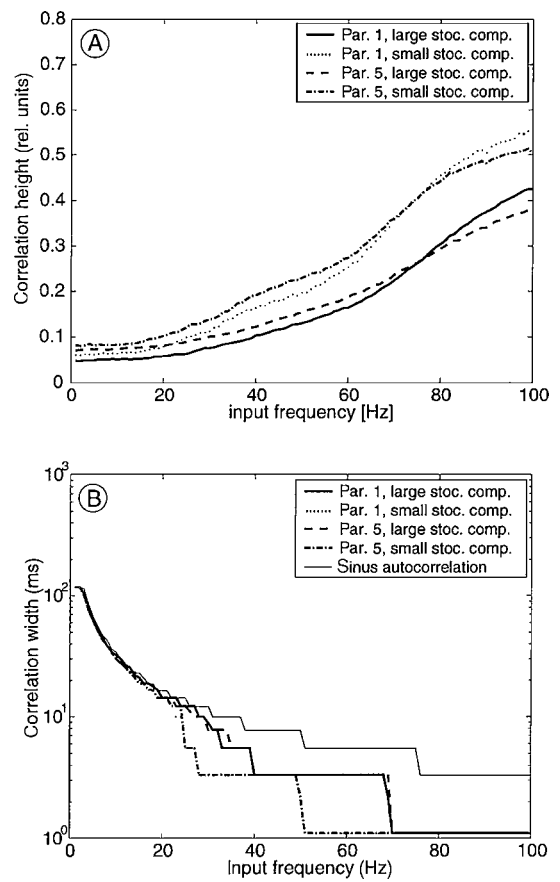


**Figure 6.** Cross-correlation analysis of spike trains elicited by sinusoidal membrane potential fluctuations. The deterministic component had the same amplitude and mean as described in the legend of Fig. 5. Its frequency was increased in steps of 1 Hz. The variance of the stochastic fluctuations had either the same (large stoc. comp., variance  $2.8 \text{ mV}^2$ ) or half the size (small stoc. comp., variance  $1.4 \text{ mV}^2$ ) of that determined for HS-cell responses. 500 individual responses each lasting 2.96 s were evaluated for the standard parameter set 1 (see Table 1) and for parameter set 5 that does not explicitly include the influence of membrane potential changes  $\rho(t) = 0$ . **A:** The correlation height (peak height above chance level of spike coincidences) grows with increasing frequency of the input signal for both amplitudes of the stochastic membrane potential component and for all parameter sets. There are moderate quantitative differences between the simulations with different parameter values. Variations of the amplitude of the noise have a stronger effect on the correlation height than variations of the model parameters. **B:** The correlation width falls steeply within the low-frequency range for both amplitudes of the stochastic component and all parameter sets. The results are nearly identical for the different parameter sets and a given noise level. The correlation width decreases in discrete steps corresponding to the binwidth of 1.1 ms. The thin solid line indicates the width of the autocorrelation of the deterministic sinusoidal input fluctuations. For frequencies above approximately 20 Hz the crosscorrelation of the spike trains is narrower for both levels of stochastic fluctuations than the autocorrelation of the sinusoidal input.

of the stochastic component, the height and width of the cross-correlogram depend on the frequency of the deterministic membrane potential fluctuations: The correlation height increases with increasing input frequency (Fig. 6A), whereas the correlation width decreases (Fig. 6B). To assess the precision of time-locking of spikes to the membrane potential fluctuations, the width of the correlation peak of the spike trains was compared to the width of the autocorrelogram of the corresponding sinusoidal membrane potential fluctuations (Fig. 6B). For frequencies below approximately 20 Hz the width of the spike correlograms and the sinus autocorrelogram are essentially the same. This similarity indicates that the spike rate follows the membrane potential changes and individual spikes do not time-lock to a given phase. In contrast, for higher frequencies the correlation width of the simulated spike trains becomes smaller than the width of the autocorrelation of the sinusoidal input. Hence, for frequencies above 20 Hz spikes are time-locked more precisely to the input fluctuations than would be expected if the instantaneous spike rate were proportional to the instantaneous membrane potential.

The exact values of correlation height and width depend on the size of the stochastic membrane potential fluctuations that are superimposed on the sinusoidal input (Fig. 6). For increasing size of the stochastic component, higher frequencies of the deterministic membrane potential fluctuations are needed to obtain a given correlation height and width. Nevertheless, the dependence between input frequency and correlation height and width are qualitatively the same for different sizes of the stochastic membrane potential component. The correlation between spike trains elicited by the same sinusoidal input superimposed by different stochastic components with the same statistical properties is also influenced by the shape of the power spectrum of the stochastic component and by the amplitude of the sinusoidal input. These effects have not been analyzed systematically in the present study.

How robust are these conclusions with respect to variations of the model parameters? Changes in the parameters that determine the refractory period ( $\gamma^{ref}$  and  $\eta_0$ ) affect the shape of the correlogram of spike responses to a sinusoidal membrane potential input much more than changes in the other model parameters. Due to the fact that the refractory period interacts with the periodicity of the deterministic input, the shape of the correlogram depends on the refractory period in a complex manner. In contrast, correlation height and

width do not depend much on those parameters that determine the dependence of the spike threshold on the membrane potential changes ( $T$  and  $\rho_0$ ; compare data obtained with parameter sets 1 and 5 in Fig. 6). For frequencies below approximately 75 Hz the correlation height is slightly larger, when the membrane potential changes do not explicitly influence the spike threshold (parameter set 5). For frequencies above about 75 Hz this relationship reverses (Fig. 6A). This reversal is plausible as spikes are expected to time-lock even better to fast membrane potentials when the influence of membrane potential changes is explicitly modeled (parameter set 1) than when it is not (parameter set 5). Since for the low-frequency input all fast membrane potential changes are stochastic, this feature of parameter set 1 reduces the correlation height compared to parameter set 5. However, in the high-frequency range spikes can time-lock to the deterministic input more precisely when the fast membrane potential changes influence the spike threshold explicitly. Therefore, for deterministic input with sufficiently high frequencies the correlation height is larger for parameter set 1 than for parameter set 5. The correlation width was virtually not affected by the parameter changes (Fig. 6B). For neurons with a realistic amount of stochastic membrane potential fluctuations it can be concluded that independent of the parameter choice relatively fast membrane potential changes are necessary to time-lock spikes precisely. This result is in accordance with a previous conclusion based on experimental data on fly motion-sensitive neurons (Warzecha et al., 1998).

### 3.3. *Dependence of Spike Synchronization on the Amount of Common Input*

So far the model has been used to simulate spike trains elicited in a neuron by repetitive identical stimulation superimposed by noise. Successive spike trains simulated by using the same deterministic membrane potential fluctuations but different stochastic response components can also be interpreted as spike trains elicited simultaneously in neurons with identical properties that share parts of their input signals. As in many other systems (see Section 1, Introduction), two spiking neurons in the fly motion pathway (H1 and H2) generate a large proportion of their spikes synchronously (Warzecha et al., 1998). These motion-sensitive interneurons are thought to receive their input signals from largely the same population of presynaptic elements. An example

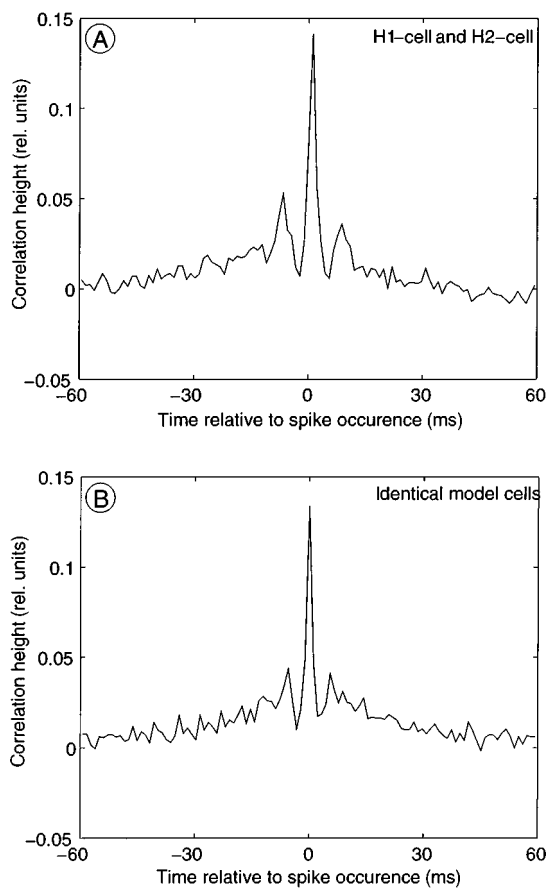


**Figure 7.** Cross-correlograms of simultaneously recorded and simulated neurons. Zero level indicates level of random coincidences of spikes. **A:** Cross-correlogram of simultaneously recorded responses of the H1-cell and the H2-cell to white-noise velocity fluctuations. 30 responses each lasting 3.1 s were used (modified from Warzecha et al., 1998). **B:** Cross-correlogram of responses of two identical model neurons. The input to the model cells consisted of the stimulus-induced membrane potential obtained from an HS-cell that was superimposed by stochastic fluctuations with the variance ( $2.8 \text{ mV}^2$ ) and the power spectrum fitted to experimental data (see Section 2, Methods). The stochastic input consisted of two components, one common to both neurons and one component that was generated independently for both neurons. The variance of both stochastic components was identical ( $C = 50\%$  common stochastic input). 30 pairs of simulated spike trains each lasting 2.96 s were evaluated.

for a cross-correlogram of their spike trains is given in Fig. 7A. The sharp peak in the cross-correlogram can be reproduced by two model cells with identical properties (Fig. 7B).

The model enables us to analyze which aspects of the spike-generation mechanism are important determinants of spike synchronization in pairs of cells and

to investigate how the temporal precision of spike generation depends on the composition of the input signals. In the first step of the analysis, two cells with identical parameters were simulated. Both cells shared as deterministic component the same stimulus-induced membrane potential as obtained from a fly motion-sensitive neuron during motion stimulation with white-noise velocity fluctuations. The stochastic component of the membrane potential consisted of two parts—one part common to both cells, the other one statistically independent for each cell (see Section 2, Methods). The relative size of these stochastic components was varied, while the variance of the total stochastic input was kept constant. The power spectra of the stochastic components were the same (except for a linear scale factor) but different from that of the deterministic component. In particular, the stochastic components contained more power at high frequencies than the deterministic component (see Section 2, Methods, and Fig. 3). The similarity of spike trains of pairs of neurons was quantified by cross-correlation analysis. When spike trains are simultaneously recorded, the height of the cross-correlogram at  $t = 0$  above the chance level of spike coincidences can indicate the amount of synchronous activity. The width at half-height is taken to quantify the temporal precision. The correlogram peak is small and very broad if there is no common stochastic input to the two simulated cells and the only common membrane potential changes are stimulus-induced (Fig. 8). The width of the cross-correlogram decreases (Fig. 8A) and its height increases (Fig. 8B) with increasing percentage  $C$  of common stochastic input. The correlation width falls steeply until the common stochastic input reaches 50%. For larger common stochastic input the correlation has a narrow peak that indicates spike synchronization on a millisecond timescale. The correlation height rises only slightly as long as the independent part is predominant. Only when the common stochastic component gets larger than the independent one, the correlation height rises steeply and reaches its maximum for 100% common input. A qualitatively similar result was obtained with a reduced version of our model in which the threshold was kept constant apart from an absolute refractory period (data not shown) as well as with integrate-and-fire units that share part of their input consisting of Poisson spike trains (Ritz and Sejnowski, 1997; Shadlen and Newsome, 1998).

To analyze the role of different model parameters for the correlation between the spike trains of two identical model neurons the parameters were varied

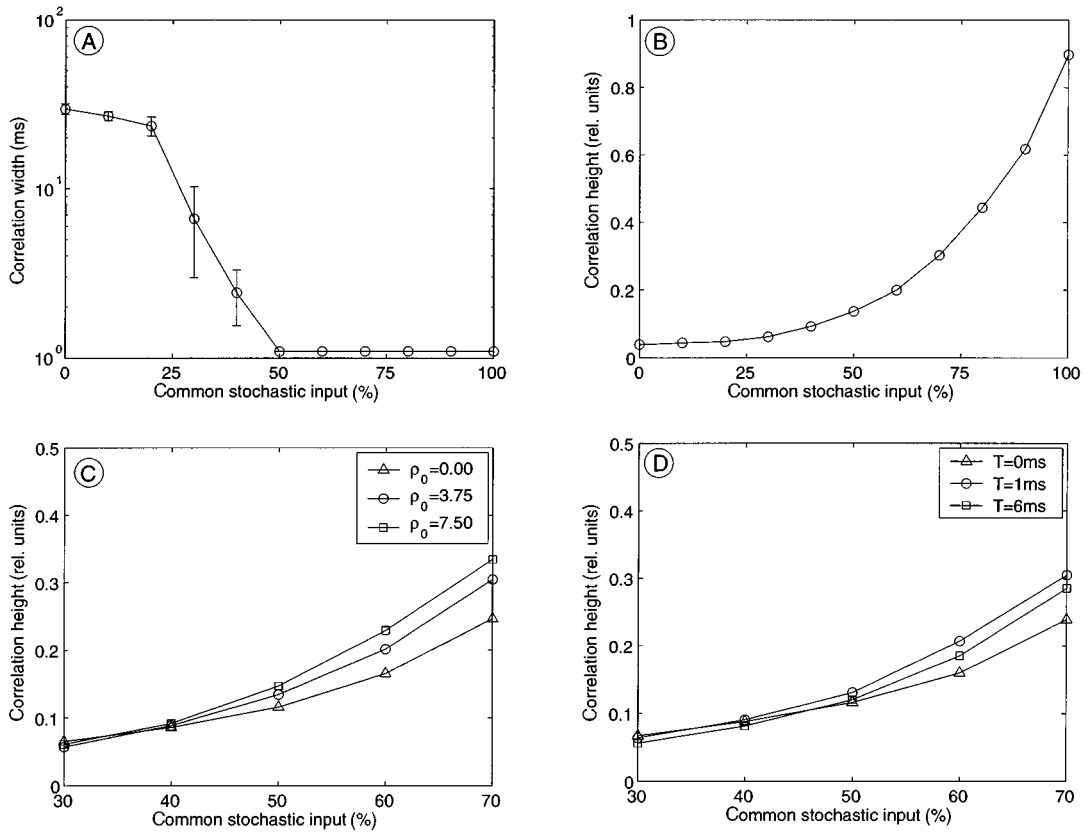


**Figure 8.** Correlated activity of pairs of neurons depends on the percentage of common stochastic input. The input common to two identical model neurons consisted of the deterministic membrane potential component and a stochastic component that was identical for both neurons but different from trial to trial. In addition, each model neuron was fed with stochastic membrane potential fluctuations generated independently from those of the other neuron. The proportion of common and independent stochastic input (see Section 2, Methods) was varied while the total variance of the input was held constant. The stochastic component of the input had more power than the deterministic component for frequencies above about 30 Hz. 10 simulations were evaluated, each consisting of 100 responses of 2.96 s duration. The results of all simulations were averaged. **A, B:** The correlation width decreases and the correlation height grows with increasing percentage  $C$  of the common stochastic input. The correlation height must stay below 1 because it is calculated as the height above the chance level of spike coincidences. Error bars in A denote SEMs of correlation widths of 10 simulations. The SEMs of correlation heights are smaller than the range covered by the symbols. **C, D:** Comparison of correlation heights for pairs of identical model cells with different parameter values. The circles are a detail of B calculated with parameter set 1. The other symbols indicate the outcome of simulations using the same parameter set except for  $\rho_0$  in C and  $T$  in D. Triangles show simulations in which membrane potential changes are not taken into account in determining the spike threshold ( $\rho(t) = 0$ ). **C:** For a given percentage of common stochastic input the correlation height is largest when changes in the membrane potential are allowed to affect the threshold most strongly. **D:** Highest correlation peaks were obtained for short integration times. As in C the correlations are smallest when the influence of membrane potential changes is not explicitly taken into account (triangles).

systematically. Only two of the five model parameters were found to influence the correlation in a noticeable way. In contrast to the findings obtained with sinusoidally fluctuating input, parameters determining the refractoriness do not much influence the correlation. Instead, enlarging the weight  $\rho_0$  with which membrane potential changes affect spike threshold increases the correlation height (Fig. 8C). For higher values of  $\rho_0$  than those used in Fig. 8C the correlation height

increases even further. The correlation height is largest for short time windows  $T$  within which the membrane potential changes are determined (Fig. 8D). When the membrane potential changes are not taken into account ( $T = 0$  or  $\rho_0 = 0$ ), the correlation height for a given amount of common input is smaller than for the standard model (compare triangles and circles in Fig. 8C and D). For longer integration times  $T$  than those employed in Fig. 8D the correlation height decreases,

approaching the values obtained for  $T = 0$ . Nevertheless, the dependence of the correlation height on the percentage of common stochastic input stays qualitatively the same for all parameter sets.

So far, we used the same parameters to simulate two neurons. However, most biological neurons exhibiting synchronized spike activity are unlikely to be identical. When any of the model parameters differed for the two simulated neurons, the correlation height decreased for a given percentage of the common stochastic membrane potential. This implies that for neurons simulated with different parameter sets a larger percentage of common stochastic input is needed than for identical model neurons to obtain a given correlation height and width. Especially for simulations without influence of the membrane potential changes on the spike threshold ( $T = 0$  or  $\rho_0 = 0$ ), the relative size of the common stochastic input must be increased considerably to maintain a given correlation height. These findings imply that the level of common noise that is needed to explain synchronized activity of pairs of neurons is underestimated if the estimation is based on model cells simulated with the same parameter set. As has been shown above, the degree of synchronization found in a pair of fly motion-sensitive neurons (H1 and H2) can be reproduced by a pair of identical model cells when they share 50% of their stochastic input (Fig. 7). The real level of common stochastic input can be expected to be much larger because both neurons have divergent characteristic properties (such as mean spike rates differing by a factor of 2 to 3) and thus require different parameter sets to account for these properties. For any parameter set chosen to fit the different average spike activities of H1 and H2, at least 65% common stochastic input was needed to obtain cross-correlograms with a height and width similar to the experimental data. For several parameter sets correlation peaks were small and broad even when the total stochastic component was common to both cells.

#### 4. Discussion

The variability of spike trains and the time-locking of spikes to membrane potential fluctuations has been simulated with a time-dependent threshold model of spike generation. It has been shown that spikes are mainly time-locked to rapid depolarizations of the membrane potential rather than to its slowly changing components. This characteristic of spike generation will be discussed with respect to (1) the features of the

model of spike generation that are responsible for it and (2) its functional consequences for the synchronization of spikes in neurons with common input and for the encoding of time-dependent sensory stimuli.

##### 4.1. *Relevant Features of the Model of Spike Generation*

The time-dependent threshold model of spike generation proposed in the present study is a phenomenological model with parameters adjusted to fit the spike responses of a fly motion-sensitive neuron. Spike activity in fly motion-sensitive neurons has already been simulated by different model approaches ranging from special versions of the integrate-and-fire model (Mastebroek, 1974; Gestri et al., 1980) to a single-compartment Hodgkin-Huxley type neuron (Haag et al., 1999). None of these models was appropriate for our purposes. Whereas the models of Mastebroek (1974) and Gestri et al. (1980) were developed to account for general statistical properties of averaged spike trains, we wanted to explain the timing of individual spikes. In Hodgkin-Huxley type models currents serve as input to the spike-generation mechanism, whereas we wanted to feed the spike-generation mechanism with membrane potential changes elicited by dynamic motion stimuli because these, rather than the corresponding currents, are available for fly motion-sensitive neurons from electrophysiological experiments.

To account for the variability of spike trains as it arises due to random background synaptic activity and stochastic opening and closing of ion channels and to a lesser extent to thermal noise (Manwani and Koch, 1999a, 1999b), a stochastic component must be included into any spike-generation model. We added stochastic fluctuations to the deterministic component of the membrane potential (see also Reich et al., 1998). An implicit assumption of this approach was that noise is independent of the stimulus. This assumption does not necessarily hold for real neurons. A recent study revealed that the stochastic membrane potential component in the H1-neuron of the fly may depend on the stimulus conditions (Warzecha et al., 2000). Although the implications of this finding for the mechanism of spike generation need further investigations, the qualitative results of our model study do not critically depend on the assumption of stimulus-independent noise.

There are further possibilities to introduce stochasticity. In some models the membrane potential

determines at each instant of time the probability for eliciting a spike. In this way the stochastic nature of spike generation is simulated (e.g., Gerstner and van Hemmen, 1992; Heck et al., 1993; Warzecha et al., 1998). In other models a stochastically changing spike threshold was used (e.g., Mastebroek, 1974; Reich et al., 1997). Formally, the same output spike trains are obtained when stochastic fluctuations are added to the threshold or to the membrane potential because the *difference* between the actual threshold and the membrane potential determines whether or not a spike is generated. We used stochastic membrane potential fluctuations and a deterministic (but time-varying) threshold (e.g., Cecchi et al., 2000) because there is evidence that the spike-generation process does not represent the main source of variability of neural activity (Mainen and Sejnowski, 1995; Zador, 1998; Stevens and Zador, 1998). For integrate-and-fire units the threshold is often assumed to be constant, and a stochastic spike output is obtained by using stochastic spike trains as input (e.g., Shadlen and Newsome, 1998; Koch, 1999).

The relative refractory period is an absolute necessity in our spike-generation model to explain the spike responses of fly motion-sensitive neurons. Since the relative refractory period is a well established property of spike generation (e.g., Kandel et al., 1995), it is not surprising that it was explicitly taken into account in many phenomenological models of spike generation (e.g., Mastebroek, 1974; Eckhorn et al., 1990; Gerstner and van Hemmen, 1992; Heck et al., 1993). In contrast, in the Hodgkin-Huxley model of spike-generation (Hodgkin and Huxley, 1952) refractoriness is not an explicit model parameter but derives from the dynamics of the spike mechanism itself.

It is well established that fast depolarizing currents injected into a neuron trigger a spike at more negative voltage values than do slowly depolarizing currents (e.g., Johnston and Wu, 1995). This fundamental feature of spike generation is reflected in the experimental finding that spikes couple to rapid membrane potential fluctuations more reliably than to less transient ones (Mainen and Sejnowski, 1995; Haag and Borst, 1996; Reich et al., 1997; Mechler et al., 1998; Warzecha et al., 1998). Moreover, the timing of spikes could be predicted better if the time derivative of the membrane potential, rather than the actual membrane potential itself, is assumed to determine the spike threshold (Ebbinghaus et al., 1997). These results are consistent with the phase advance of the peak in the PSTH with respect to sinusoidal membrane potential fluctuations (Fig. 5)

and the increased phase locking of spikes to higher frequencies (Fig. 6). With phenomenological models of spike generation, a more precise coupling to rapid membrane potential fluctuations than to slow ones is obtained even if the spike threshold is not *explicitly* influenced by membrane potential changes (Fig. 6; see also Cecchi et al., 2000). Nonetheless, as was shown by the present model simulations the explicit influence of membrane potential changes on spike threshold influences the precision of time-locking of individual spikes to the synaptic input of the cell. In particular, if the membrane potential dynamics affects the spike threshold, a smaller amount of common stochastic input is needed to explain synchronous spike activity than when the spike threshold is not affected in this way.

#### 4.2. Significance of Fast Membrane Potential Fluctuations

A large part of the membrane potential fluctuations of a neuron is due to its synaptic input (Calvin and Stevens, 1968). Spikes tend to time-lock to the fast rather than to the slow components of these fluctuations (see above). Such fast membrane potential changes may be tightly time-locked to changes in sensory stimuli, or they may be unrelated to the temporal properties of the stimulus. How well spikes couple to a sensory stimulus depends on the proportion of the amplitudes and on the frequency composition of the stimulus-induced and of the stochastic membrane potential component. Only if the amplitude of the stimulus-induced component exceeds the stochastic component in a sufficiently high-frequency range can spikes be time-locked precisely to the stimulus. Nevertheless, synchronized spike activity can appear even if the stimulus does not determine the exact timing of spikes (e.g., Usrey et al., 1998; Usrey and Reid, 1999; Warzecha et al., 1998). Hence, rapid membrane potential fluctuations in different neurons that have their origin in a source common to these neurons may lead to synchronized spike activity regardless of whether the rapid fluctuations are induced by the stimulus or whether they are unrelated to it. Accordingly, it cannot be concluded from the occurrence of spike synchronization that this synchronization is important for the computations a neuronal system performs. Instead, it has to be analyzed for the respective system whether synchronized activity is used by neurons at the next processing stage and whether the exact timing of spikes plays a functional role to encode sensory stimuli.

#### 4.2.1. Dependence of Spike Timing on Sensory Stimulation.

On what time scale spikes of sensory neurons are coupled to sensory stimuli is constrained by the temporal properties of the underlying stimulus-induced membrane potential fluctuations and, thus, by the temporal properties of the respective stimulus. This time scale can range over several orders of magnitude depending on the system under consideration. For instance, in the electrosensory system of electric fish phase-coding neurons are known that fire one spike phase-locked with very little temporal jitter to each cycle of the electric organ discharge (Heiligenberg, 1991; Kawasaki, 1997). In the auditory system, interaural time differences are used to localize sound sources. This task can be solved only if very precise phase-locking of the individual spikes to the arrival times of the sound at the two ears is guaranteed (Carr and Friedmann, 1999). In contrast, spikes of motion-sensitive neurons in visual systems usually lock to motion stimuli on a coarser timescale. This is because high-frequency changes in the direction of motion are attenuated as a consequence of motion computations (e.g., Egelhaaf and Borst, 1993). Due to these computational constraints, mainly relatively low frequencies (up to 20 to 40 Hz) dominate the stimulus-induced responses of motion-sensitive neurons—for example, in the monkey and the fly when activated with broad-band velocity fluctuations (Bair and Koch, 1996; Haag and Borst, 1997, 1998; Warzecha et al., 1998). For the fly it was shown that for these stimulus conditions the power of the stochastic membrane potential component exceeds the power of the deterministic fluctuations for frequencies above about 30 Hz. Hence most spikes of the motion-sensitive H1-cell were concluded to time-lock with a millisecond precision to the fast stochastic rather than to the stimulus-induced response component (Warzecha et al., 1998).

The dynamical properties of the stimulus-induced response component need to be qualified because they were obtained with artificially generated stimuli that may differ from natural stimuli in their amplitude and their frequency composition. Both of these aspects may influence the power spectrum of the stimulus-induced response component and thus the precision with which spikes can couple to the visual stimulus. In specific behavioral situations the retinal image velocities that are encountered by flies can assume very large values (e.g., Land and Collett, 1974; Wagner, 1986). In contrast to a recent hypothesis (de Ruyter van Steveninck et al., 2000), the response

amplitude of motion-sensitive neurons in a variety of species (Pollen et al., 1978; Wolf-Oberhollenzer and Kirschfeld, 1990; Lisberger and Movshon, 1999) including the fly (Hausen, 1982; Maddess and Laughlin 1985, Egelhaaf and Reichardt, 1987) does not scale proportionally to stimulus velocity. In particular, during white-noise velocity stimulation as used in the present account (such as Figs. 2 and 3) the membrane potential of fly motion-sensitive neurons de- and hyperpolarized by about 10 mV. Much larger response amplitudes cannot be elicited close to the output region of the motion-sensitive neurons in the fly's brain by any visual motion stimulation. Therefore, it seems unlikely that due to the large amplitude of the retinal image velocities that occur in certain behavioral situations, the stimulus-induced component will exceed the stochastic component in the high-frequency range.

The frequency composition of the stimulus (when an animal is confronted with a behaviorally relevant situation) largely depends on the animal's behavior. For instance, if a fly tries to fly straight and to stabilize its flight course against disturbances, the retinal velocity was found in behavioral studies in a flight simulator to change only relatively slowly (Warzecha and Egelhaaf, 1996). The resulting membrane potential changes are not fast enough to time-lock spikes with a millisecond precision (Warzecha and Egelhaaf, 1997). On the other hand, during very fast saccade-like body turns (see, e.g., van Hateren and Schilstra, 1999; Schilstra and van Hateren, 1999), transient image displacements may occur that elicit postsynaptic membrane potentials fast enough to time-lock spikes precisely (Warzecha and Egelhaaf, 2000; de Ruyter van Steveninck et al., 2000). In conclusion, it very much depends on the stimulus conditions and thus on the behavioral context as well as the biophysical, and computational constraints, on what time scale spikes time-lock to sensory stimuli under natural conditions.

#### 4.2.2. Implications for Neural Coding.

Our results hint at a novel perspective with respect to the apparent antagonism between rate code and time code (see, e.g., Shadlen and Newsome, 1994; Softky, 1995). On the one hand, spikes time-lock precisely to high-frequency membrane potential fluctuations. Their timing is then more precise than the underlying membrane potential dynamics,—that is, the spike rate is not proportional to the membrane potential as is the case for slow membrane potential changes (Fig. 5). Hence, fast depolarizations of the cell are a prerequisite for a code that

transmits information by the exact timing of individual spikes and for synchronizing the activity of neurons with common input on a fine timescale. On the other hand, slow stimulus-induced membrane potential changes determine the probability of spike timing only on a coarse time scale, at least if these are superimposed by noise. Hence, slowly changing stimuli on their own do not synchronize the activity of neurons that share parts of their inputs. Instead, such stimuli are encoded by the spike rate, whereas the exact timing of the individual spikes is determined by fast stochastic processes. However, these two kinds of coding are not strictly separate since rate coding may turn into time coding and vice versa, when the dynamics of the membrane potential fluctuations changes. Accordingly, the relevance of spike timing for encoding a stimulus is not a question that can be answered with yes or no. To what extent the timing of individual spikes matters rather depends on the dynamics of the membrane potential changes of the investigated neuron that are induced by the stimulus, on the one hand, and the stochastic membrane potential component, on the other hand.

### Acknowledgments

We thank our coworkers R. Kern, H. Krapp, R. Kurtz, and J.P. Lindemann for reading and discussing the manuscript. The detailed constructive comments of two anonymous referees are gratefully acknowledged. This study was supported by a grant of the Studienstiftung des deutschen Volkes to J.K. and by the DFG.

### References

- Alonso JM, Usrey W, Reid R (1996) Precisely correlated firing in cells of the lateral geniculate nucleus. *Nature* 383:815–819.
- Bair W (1999) Spike timing in the mammalian visual system. *Curr. Opin. Neurobiol.* 9:447–453.
- Bair W, Koch C (1996) Temporal precision of spike trains in extrastriate cortex of the behaving macaque monkey. *Neural Comput.* 8:1185–1202.
- Berry MJ, Warland DK, Meister M (1997) The structure and precision of retinal spike trains. *PNAS, USA* 94:5411–5416.
- Bialek W, Rieke F (1992) Reliability and information transmission in spiking neurons. *TINS* 15:428–434.
- Britten K, Shadlen M, Newsome W, Movshon J (1993) Responses of neurons in macaque MT to stochastic motion signals. *Vis. Neurosci.* 10:1157–1169.
- Brivanlou I, Warland D, Meister M (1998) Mechanisms of concerted firing among retinal ganglion cells. *Neuron* 20:527–539.
- Brody C (1999) Correlations without synchrony. *Neural Comput.* 11:1537–1551.
- Buračas G, Zador A, DeWeese M, Albright T (1998) Efficient discrimination of temporal patterns by motion-sensitive neurons in primate visual cortex. *Neuron* 20:956–969.
- Calvin W, Stevens C (1968) Synaptic noise and other sources of randomness in motoneuron interspike intervals. *J. Neurophysiol.* 31:574–587.
- Carr C, Friedmann M (1999) Evolution of time coding systems. *Neural Comput.* 11:1–20.
- Cecchi G, Sigman M, Alonso JM, Martinez L, Chialvo D, Magnasco M (2000) Noise in neurons is message-dependent. *Proc. Natl. Acad. Sci. USA* 97:5557–5561.
- de Ruyter van Steveninck R, Bialek W (1988) Real-time performance of a movement-sensitive neuron in the blowfly visual system: Coding and information transfer in short spike sequences. *Proc. R. Soc. Lond. B* 234:379–414.
- de Ruyter van Steveninck R, Bialek W (1995) Reliability and statistical efficiency of a blowfly movement sensitive neuron. *Phil. Trans. R. Soc. Lond. B* 348:321–340.
- de Ruyter van Steveninck R, Borst A, Bialek W (2000) Real-time encoding of motion: Answerable questions and questionable answers from the fly's visual system. In: Zanker JM, Zeil J, eds. *Visual Motion*. Springer, Heidelberg (in press).
- Ebbinghaus C, Diesmann M, Rotter S, Aertsen A (1997) The neural firing threshold: Can I help U? In: Elsner N, Wässle H, eds. *Göttingen Neurobiology Report 1997. Proceedings of the 25th Göttingen Neurobiology Conference 1997*. Thieme, Stuttgart p. 624.
- Eckhorn R, Reitboeck H, Arndt M, Dicke P (1990) Feature linking via synchronization among distributed assemblies: Simulations of results from cat visual cortex. *Neural Comput.* 2:293–307.
- Egelhaaf M, Borst A (1993) Movement detection in arthropods. In: Miles FA, Wallman J, eds. *Visual Motion and Its Role in the Stabilization of Gaze*. Elsevier, Amsterdam. pp. 53–77.
- Egelhaaf M, Reichardt W (1987) Dynamic response properties of movement detectors: Theoretical analysis and electrophysiological investigation in the fly system of the fly. *Biol. Cybern.* 56:69–87.
- Egelhaaf M, Warzecha, A-K (1999) Encoding of motion in real time by the fly visual system. *Curr. Opin. Neurobiol.* 9:454–460.
- Gerstner W, van Hemmen L (1992) Associative memory in a network of “spiking” neurons. *Network* 3:139–164.
- Gestri G, Mastebroek H, Zaagman W (1980) Stochastic constancy, variability and adaptation of spike generation: Performance of a giant neuron in the visual system of the fly. *Biol. Cybern.* 38:31–40.
- Haag J, Borst A (1996) Amplifications of high-frequency synaptic inputs by active dendritic membrane processes. *Nature* 379:639–641.
- Haag J, Borst A (1997) Encoding of visual motion information and reliability in spiking and graded potential neurons. *J. Neurosci.* 17:4809–4819.
- Haag J, Borst A (1998) Active membrane properties and signal encoding in graded potential neurons. *J. Neurosci.* 18:7972–7986.
- Haag J, Vermeulen A, Borst A (1999) The intrinsic electrophysiological characteristics of fly lobula plate tangential cells: III. Visual response properties. *J. Comp. Neurosci.* 7:213–234.

- Hausen K (1981) Monocular and binocular computation of motion in the lobula plate of the fly. *Verh. Dtsch. Zool. Ges.* 74:49–70.
- Hausen K (1982) Motion sensitive interneurons in the optomotor system of the fly. II. The horizontal cells: Receptive field organization and response characteristics. *Biol. Cybern.* 46:67–79.
- Heck D, Rotter S, Aertsen A (1993) Spike generation in cortical neurons: Probabilistic threshold function shows intrinsic and long-lasting dynamics. In: Aertsen A, ed. *Brain Theory*. Elsevier, Amsterdam. pp. 241–249.
- Heiligenberg W (1991) *Neural Nets in Electric Fish*. MIT Press, Cambridge, MA.
- Hengstenberg R (1982) Common visual response properties of giant vertical cells in the lobula plate of the blowfly *Calliphora*. *J. Comp. Physiol.* 149:179–193.
- Hodgkin A, Huxley A (1952) A quantitative description of ion currents and its applications to conduction and excitation in nerve membranes. *J. Physiol. (London)* 117:500–544.
- Johnston D, Wu SS (1995) *Foundations of Cellular Neurophysiology*. MIT Press, Cambridge, MA.
- Kandel E, Schwartz J, Jessell T (1995) *Essentials of neural science and behavior*. Appleton & Lange, Norwalk, CT.
- Kawasaki M (1997) Sensory hyperacuity in the jamming avoidance response of weakly electric fish. *Curr. Opin. Neurobiol.* 7:473–479.
- Koch C (1999) *Biophysics of Computation: Information Processing in Single Neurons*. Oxford University Press, New York.
- Lamp I, Reichova I, Ferster D (1999) Synchronous membrane potential fluctuations in neurons of the cat visual cortex. *Neuron* 22:361–374.
- Land MF, Collet TS (1974) Chasing behaviour of houseflies (*Fannia caicularis*). *J. Comp. Physiol.* 89:331–357.
- Levine M (1998) Models for the cross-correlation between retinal ganglion cells. *Biol. Cybern.* 79:367–376.
- Lisberger SG, Movshon JA (1999) Visual motion analysis for pursuit eye movements in area MT of macaque monkeys. *J. Neurophysiol.* 19:2224–2246.
- Maass W (1996) Networks of spiking neurons: The third generation of neural network models. *Neur Networks* 10:1659–1671.
- Maddess T, Laughlin SB (1985) Adaptation of the motion-sensitive neuron H1 is generated locally and governed by contrast frequency. *Proc. R. Soc. Lond. B* 225:251–275.
- Mainen Z, Sejnowski T (1995) Reliability of spike timing in neocortical neurons. *Science* 268:1503–1506.
- Manwani A, Koch C (1999a) Detecting and estimating signals in noisy cable structures: I. Neuronal noise sources. *Neural Comput.* 11:1797–1829.
- Manwani A, Koch C (1999b) Detecting and estimating signals in noisy cable structures: II. Information theoretical analysis. *Neural Comput.* 11:1831–1873.
- Mastebroek H (1974) Stochastic structure of neural activity in the visual system of the blowfly. Ph.D. thesis, Rijksuniversiteit te Groningen.
- Mechler F, Victor JD, Purpura KP, Shapley R (1998) Robust temporal coding of contrast by V1 neurons for transient but not for steady-state stimuli. *J. Neurosci.* 18:6583–6598.
- Pollen DA, Andrews BW, Feldon SE (1978) Spatial frequency selectivity of periodic complex cells in the visual cortex of the cat. *Vis. Res.* 18:665–682.
- Reich D, Victor J, Knight B (1998) The power ratio and the interval map: Spiking models and extracellular recordings. *J. Neurosci.* 18:10090–10104.
- Reich D, Victor J, Knight B, Ozaki T, Kaplan E (1997) Response variability and timing precision of neuronal spike trains in vivo. *J. Neurophysiol.* 77:2836–2841.
- Ritz R, Sejnowski T (1997) Correlation coding in stochastic neural networks. In: Gerstner W, Germona A, Hasler M, Nicaud J-D, eds. *Proceedings ICANW 97*. Springer, Heidelberg, pp. 79–84.
- Schilstra C, Hateren JH van (1999) Blowfly flight and optic flow. I. Thorax kinematics and flight dynamics. *J. Exp. Biol.* 202:1481–1490.
- Schneidman E, Freedman B, Segev I (1998) Ion channel stochasticity may be critical in determining the reliability and precision of spike timing. *Neural Comput.* 10:1679–1703.
- Shadlen M, Newsome W (1994) Noise, neural codes and cortical organization. *Curr. Opin. Neurobiol.* 4:569–579.
- Shadlen M, Newsome W (1998) The variable discharge of cortical neurons: Implications for connectivity, computation, and information coding. *J. Neurosci.* 18:3870–3896.
- Softky W (1995) Simple codes versus efficient codes. *Curr. Opin. Neurobiol.* 5:239–247.
- Softky W, Koch C (1993) The highly irregular firing of cortical cells is inconsistent with temporal integration of random epsps. *J. Neurosci.* 13:334–350.
- Stevens C, Zador A (1998) Input synchrony and the irregular firing of cortical neurons. *Nature Neurosci* 1:210–217.
- Tolhurst D, Movshon JA, Dean A (1983) The statistical reliability of signals in single neurons in cat and monkey visual cortex. *Vis. Res.* 23:775–785.
- Usrey WM, Reid RC (1999) Synchronous activity in the visual system. *Ann. Rev. Physiol.* 61:435–456.
- Usrey WM, Reppas JB, Reid RC (1998) Paired-spike interactions and synaptic efficacy of retinal inputs to the thalamus. *Nature* 395:384–387.
- van Hateren JH, Schilstra C (1999) Blowfly flight and optic flow. II. Head movements during flight. *J. Exp. Biol.* 202:1491–1500.
- Vogels R, Spileers W, Orban G (1989) The response variability of striate cortical neurons in behaving monkey. *Exp. Brain Res.* 77:432–436.
- Wagner H (1986) Flight performance and visual control of flight of the free flying housefly (*Musca domestica* L.) II. Pursuit of targets. *Phil. Trans. R. Soc. Lond. B* 312:553–579.
- Warzecha AK, Egelhaaf M (1996) Intrinsic properties of biological motion detectors prevent the optomotor control system from getting unstable. *Phil. Trans. R. Soc. Lond. B* 351:1579–1591.
- Warzecha AK, Egelhaaf M (1997) How reliably does a neuron in the visual motion pathway of the fly encode behaviourally relevant information? *Eur. J. Neurosci.* 9:1365–1374.
- Warzecha AK, Egelhaaf M (1999) Variability in spike trains during constant and dynamic stimulation. *Science* 283:1927–1930.
- Warzecha AK, Egelhaaf M (2000) Neuronal encoding of visual motion in real-time In: Zanker JM, Zeil J, eds. *Visual Motion*. Springer, Heidelberg (in press).
- Warzecha AK, Kretzberg J, Egelhaaf M (1998) Temporal precision of the encoding of motion information by visual interneurons. *Curr. Biol.* 8:359–368.

Warzecha AK, Kretzberg J, Egelhaaf M (2000) Reliability of a fly motion sensitive neuron depends on stimulus parameters. *J. Neurosci.* 20:8886–8896.

White JA, Rubinstein JT, Kay AR (2000) Channel noise in neurons. *Trends Neurosci.* 23:131–137.

Wolf-Oberhollenzer F, Kirschfeld K (1990) Temporal frequency dependence in motion-sensitive neurons of the accessory optic system of the pigeon. *Naturwiss.* 77:296–298.

Zador A (1998) Impact of synaptic unreliability on the information transmitted by spiking neurons. *J. Neurophysiol.* 79:1219–1229.